Faraday Discuss., 1994, **97**, 81–94

Improved Modelling of Atom–Molecule Potential-energy Surfaces: Illustrative Application to He–CO

Robert J. LeRoy and Carey Bissonnette†
Guelph-Waterloo Centre for Graduate Work in Chemistry, University of Waterloo, Waterloo, Ontario, Canada N2L 3G1

Thomas H. Wu, Ashok K. Dham‡ and William J. Meath
Department of Chemistry, University of Western Ontario, London, Ontario, Canada N6A 3B7

The need for better potential-energy models for atom–molecule and molecule–molecule interactions is discussed and the utility of the exchange–coulomb (XC) model is critically examined, by fitting a potential based on it to new high-resolution discrete infrared data for the He–CO Van der Waals molecule. In addition to explaining the observed spectrum as well as does an optimized empirical potential previously determined from the same data, the resulting XC surface is expected to be more realistic in regions not directly sampled by the fitted data.

Recent years have seen significant advances in our ability to simulate accurately high-resolution spectroscopic data for Van der Waals molecules and to use such simulations in automatic non-linear least-squares (ALS) fits to determine multi-dimensional potential-energy surfaces. However, as the systems studied in this way become increasingly complex, a problem of growing importance is that of devising flexible and realistic potential-energy models which do not require excessive numbers of adjustable parameters to define them. The present paper describes one such model, the exchange–coulomb or XC potential, and investigates its practical utility for defining a potential-energy surface that can represent high-resolution IR spectra of the He–CO bimer.

In the following, an outline of the nature of the problem is followed by a brief description of the nature of the observables and the computational methods used for simulating and fitting a potential to them. A version of the XC model potential suitable for rare gas (Rg)–CO interactions is then described together with details specific to He–CO. The results of fitting this model to the experimental IR data for He–CO are summarized and some of the more general aspects of this work are discussed.

Statement of the Problem

Modern studies of Van der Waals molecules began in 1964 with Watanabe and Welsh's remarkable observations of the discrete IR spectrum of the hydrogen dimer.[1] The first use of such data to test and refine models for the associated potential-energy functions followed soon after[2,3] and, within a decade, ALS fits to discrete Van der Waals molecule spectra were being used to determine full three-dimensional potential-energy surfaces for atom–diatom systems.[4] Since that time, the development of a variety of novel experimental methods has yielded a wealth of high-resolution data for a wide range of atom–

† Also: Department of Chemistry, University of Western Ontario, London, Ontario, Canada N6A 3B7.
‡ Permanent address: Department of Physics Punjabi University, Patiala-147002, India.

molecule and molecule–molecule complexes. For bimers formed between a rare-gas atom and a simple hydride (*e.g.* H_2, HX or H_2O), ALS fits to spectroscopic (and sometimes other) properties have yielded sophisticated relative-orientation dependent, and sometimes also bond-length dependent, potential-energy surfaces.[5–9] Fits to spectroscopic, vibrational predissociation and scattering data have also yielded realistic, although somewhat less precise, three-dimensional surfaces for Rg–Cl_2 complexes.[10] However, except for these two classes of systems, only a modest amount of information regarding intermolecular potentials has so far been extracted from this type of data.

For most of the past two decades, one of the main bottlenecks to full exploitation of high-quality Van der Waals molecule spectra has been the difficulty of computationally simulating the experimental data with the necessary accuracy and efficiency. However, developments in both computer technology and computational methods[11–14] are now making it readily feasible to perform very high accuracy calculations[15–17] and even ALS fits to experimental data,[18] for complexes including a heavy (*i.e.* non-hydride) rotor. It is therefore timely to address a second type of problem which threatens to limit the quality of information which may be obtained from the experimental data. This is the problem of devising a model potential-energy function which is sufficiently realistic to represent accurately all of the 'wrinkles' in the shapes of the interacting component molecules, and can reliably extrapolate to distances not directly sampled by the data, but does not require introduction of an excessive number of adjustable parameters.

In the earliest multidimensional analysis of atom–diatom spectra, the potentials were expressed as a nested product of a power series in the diatom stretching coordinate $\xi = (r - r_0)/r_0$ and Legendre series for the dependence on the relative orientation of the diatom,[4]

$$V(R, r, \theta) = \sum_{\lambda=0(2)} \sum_{k=0} \xi^k P_\lambda(\cos\theta) V_{\lambda,k}(R) \tag{1}$$

where R is the distance from the diatom centre of mass to the atom and θ is the orientation of the diatom relative to the axis R of the complex. However, while general and flexible, the expansion of eqn. (1) typically requires at least two empirical parameters for each radial strength function $V_{\lambda,k}(R)$ and, without the introduction of external constraints, even for the relatively simple H_2–Rg systems the number of parameters required to define the surface properly threatened to become excessive.[4,5]

For complexes more strongly anisotropic than those formed from H_2, use of the linear Legendre expansion of eqn. (1) is quite impractical, as the numbers of parameters required to define their angle dependence would outstrip the information content of the data long before a realistic potential form was obtained. Pack's idea of describing a potential in terms of realistic radial functions characterized by angle-dependent parameters[19] significantly reduced this problem, and has been the basis of most detailed empirical potential models for atom–molecule systems.[7–9,18] However, even for atom–diatom systems, the number of empirical parameters required grows quite rapidly. For example, in his recent determination of potential-energy surfaces for Ar–HCl and Ar–HF, Hutson required 12 empirical parameters to represent the radial and angle dependence.[7,8] For complexes formed from more elongated diatom monomers such as Cl_2 or CO, the numbers of parameters needed to define an accurate model potential of this type could be expected to far exceed the dozen required for Ar–HF, and the same will be true for all but the simplest molecule–molecule complexes.

In view of the above, it is clearly desirable to be able to build potential-energy models from components which are readily obtainable, and which also reliably represent the main features of the interaction and the shapes of the individual monomers. Recent years have seen the introduction of several such models for interactions involving closed-shell species, of which the XC[20,21] and Hartree–Fock dispersion (HFD)[22,23] models have led to state-of-the-art potentials for rare-gas interactions.[23,24] Ref. 25 pro-

vides a recent review of such potential models; additionally, the Tang and Toennies (TT) model,[26] which has many features in common with the others, is particularly noteworthy. All of these approaches combine the best available representations of the long-range interaction energy, damped at short range, with mainly repulsive terms based on Hartree–Fock calculations. However, in the HFD and TT models the repulsive term is based on 'supermolecule' calculations for the combined system, while in the XC model it is based on a calculation of the first-order coulomb and exchange energies of the interacting pair, which requires only wavefunctions for the individual component monomers (see later). Thus, the XC model promises to be the easiest to apply in general.

While originally developed for describing the pairwise interactions of rare-gas atoms, the above models have been extended and applied to interactions involving molecules.[25] However, their utility in this area has not been examined at the same critical level as in the work on the rare-gas pairs, at least in part because there exist very few reliably characterized systems on which they may be tested. The present paper therefore examines the utility of an XC model potential for explaining the recently measured IR spectrum of the He–CO complex.

Nature of the Observables and Computational Methods

A recent paper has reported measurements of high-resolution IR spectra for He–CO bimers in the 4.7 μm region near the fundamental band origin of the CO monomer, together with the determination of an anisotropic potential based on ALS fits to the observed transition frequencies.[18] Following the 'empirical model' approach described above, the coefficients of the leading dispersion and induction terms (those varying as R^{-6} and R^{-7}) were held fixed at theoretical values, and a fit to the observed line positions was used to determine angle-dependent parameters characterizing the depth and position of the potential well and the character of the short-range repulsive wall. The empirical potential thus obtained[18] was called the $V_{(3,3,3)}$ potential.

Both the positions and intensities of the discrete transitions implied by the $V_{(3,3,3)}$ potential-energy surface are in excellent agreement with experiment.[18] However, the number of truly bound states of this system is quite small, and it has a relatively large zero-point energy which places the ground-state level well above the barrier to internal rotation. Thus, there remains considerable room for uncertainty in a potential determined from this type of analysis, owing to its probable dependence on the form of the model potential used. Moreover, while it definitely greatly improved our knowledge of the well of this potential-energy surface, the reliability of this empirical potential at shorter or longer distances is open to question.

All of the calculations of eigenvalues and spectral intensities reported herein were performed using the version of the ISE method of ref. 13 applied in ref. 18. As in the analysis of ref. 18, the present potential model has no dependence on the CO bond length. However, differences between complexes formed from CO($v = 0$) and CO($v = 1$) were again accounted for by using the actual experimental CO rotational spacings to define the distances between the various channel asymptotes, and by using an additive shift to account for the fact that the levels of He–CO($v = 1$) are on average slightly more strongly bound than those of He–CO($v = 0$). Again, the intensities were calculated assuming that the overall transition dipole is entirely due to the transition dipole of the CO monomer.

In the following, the quality of the predictions generated from a given potential-energy surface is indicated by the value of the dimensionless root-mean-square deviation,

$$\mathrm{RMSD} = \sqrt{\left\{\left(\sum_{i=1}^{N_d} [Y_i(\mathrm{obs}) - Y_i(\mathrm{calc})]^2/u(Y_i)^2\right)/N_d\right\}}$$

where N_d is the number of data being fitted, Y_i(obs) and Y_i(calc) are the observed and calculated values of experimental datum number i, and $u(Y_i)$ its experimental uncertainty.

XC Model Potential for He–CO

In generating the potential model described below, the CO molecule is treated as if it were rigid, with its bond length fixed at $r = 2.14\ a_0$, a value which closely approximates the expectation value of r for the ground state of CO. Thus, the intermolecular potential is a function of the two coordinates R and θ, with $\theta = 0°$ defining the collinear alignment He–C—O. A generalized version of this potential which also depends on the CO bond length is being developed and will be presented elsewhere.

In the version of the XC model used here, the intermolecular potential is written as the sum of a scaled, mainly repulsive, short-range term, $E_{HL}^{(1)}$ and a mainly attractive term ΔE_C:

$$V(R, \theta) = FE_{HL}^{(1)}(R, \theta) + \Delta E_C(R, \theta) \tag{2}$$

where the scaling function F will be discussed later. Here, $E_{HL}^{(1)}(R, \theta) = E_{HL}(R, \theta) - E_{HL}(R = \infty, \theta)$ is the first-order Heitler–London interaction energy, which is a sum of coulomb ($E_C^{(1)}$) and exchange ($E_X^{(1)}$) contributions, where E_{HL} is evaluated from high quality Hartree–Fock wavefunctions for the isolated monomers:

$$E_{HL}(R, \theta) = \langle \hat{A}\phi_{He}\,\phi_{CO} \,|\, \hat{H}_e \,|\, \hat{A}\phi_{He}\,\phi_{CO}\rangle / \langle \hat{A}\phi_{He}\,\phi_{CO} \,|\, \hat{A}\phi_{He}\,\phi_{CO}\rangle \tag{3}$$

Here $\hat{H}_e$ is the clamped-nuclei Hamiltonian operator for He–CO, and the antisymmetrizer operator $\hat{A}$ ensures that $\hat{A}\phi_{He}\,\phi_{CO}$ is antisymmetric with respect to the interchange of electrons between He and CO.

The second term in eqn. (2) is a model for $[E_C - E_C^{(1)}]$, where E_C is the total coulomb interaction energy. It is represented by an overall corrected and individually damped dispersion plus induction multipole series:

$$\Delta E_C(R, \theta) = -G_{10}(R, \theta) \sum_{n=6}^{10} f_n(R, \theta) C_n(\theta)/R^n \tag{4}$$

Here, the individual damping functions $f_n(R, \theta)$ take account of charge overlap effects neglected in the conventional multipolar expansion,[27,28] while the 'corrector' function $G_{10}(R)$ is introduced to account for higher-order effects not explicitly represented in the model.[20,21,25] As in previous work with the XC potential, these quantities are defined by mapping accurate representations of them determined for the prototypical non-bonded $H_2(^3\Sigma_u^+)$ interaction[20–22] onto the range of the present potential *via* the scaling parameter $S = [R_e^{ref}/R_e(\theta)]$, where $R_e^{ref} = 7.82\ a_0$ is the equilibrium distance of the $H_2(^3\Sigma_u^+)$ potential, and $R_e(\theta)$ the position of the minimum in the present potential at angle θ. The values of $R_e(\theta)$, and hence of $S = S(\theta)$, are determined iteratively once the rest of the potential has been specified;[20,24] the dependence of this factor on θ introduces the anisotropy into the corrector and damping functions.[25] In particular,[21,28]

$$G_{10}(R, \theta) = 1 + 41.34 \exp(-0.8588SR) \tag{5}$$

$$f_n(R, \theta) = \{1 - \exp[-A_n SR - B_n(SR)^2 - D_n(SR)^3]\}^n \tag{6}$$

For $n = 6$, 8 and 10, the constants A_n, B_n and D_n were taken from ref. 28, while for $n = 7$ and 9 they were generated by assuming, following ref. 29, that $f_n = [f_{n-1}\, f_{n+1}]^{1/2}$ (these constants are listed in the Appendix). Note too that for each value of n, the induction-energy damping function is assumed to be the same as that for the dispersion term. This is not unreasonable in view of the dominance of the dispersion terms for the Rg–CO

interactions,[30] and the fact that little is known about induction damping functions for interactions involving molecules with diffuse charge distributions.

The long-range multipolar interaction energy coefficients $C_n(\theta)$ appearing in eqn. (4), which contain both dispersion and induction contributions, are expanded as

$$C_n(\theta) = \sum_{\lambda=0}^{n-4} C_n^{(\lambda)} P_\lambda(\cos\theta) \tag{7}$$

where the coefficients $C_n^{(\lambda)} = 0$ when $(n + \lambda)$ is odd. The induction and dispersion energy coefficients for $n \leqslant 8$ were taken from recent many-body perturbation theory (MBPT) results,[30] except that the dispersion contributions to $C_6^{(0)}$ and $C_6^{(2)}$ were replaced by the more reliable values obtained by constrained dipole oscillator strength techniques,[31] and all induction coefficients depending on the dipole moment of CO were renormalized to correspond to the experimental value[32] $Q_1 = -0.048\ ea_0$ (since the *ab initio* value is almost a factor of four too large[30]). The $C_n^{(\lambda)}$ coefficients for $n > 8$ were represented by the older MBPT results of ref. 33. The resulting set of composite coefficients, together with their estimated uncertainties, are listed in the Appendix.

The Heitler–London energies used here were computed using the CADPAC[34] implementation of the Hayes–Stone perturbation theory program,[35] with monomer SCF wavefunctions ϕ_{He} and ϕ_{CO} calculated using CADPAC with basis sets constructed from cartesian Gaussian primitives. An SCF wavefunction for He was obtained[36] using the 16s basis set of Schmidt and Ruedenberg,[37] and yields an SCF energy which is within 2×10^{-5}% of the exact Hartree–Fock value. The standard CADPAC (8s6p3d) basis sets for the C and O atoms, which consist of a contraction of the Van Duijneveldt (13s8p) bases[38] to (8s6p) plus three sets of d primitives, were used to compute an SCF wavefunction for CO at $r = 2.14\ a_0$. This wavefunction has an SCF energy of $-112.7863\ E_h$, and dipole (Q_1), quadrupole (Q_2) and octapole (Q_3) moments of $0.112\ ea_0$, $-1.542\ ea_0^2$ and $-3.746\ ea_0^3$, respectively, values quite similar to those obtained from accurate numerical HF calculations for CO at $r = 2.132\ a_e$.[39] For comparison, the recent correlated *ab initio* calculations of Hettema *et al.*[30] yield $Q_1 = -0.186\ ea_0$, $Q_2 = -1.524\ ea_0^2$ and $Q_3 = -3.879\ ea_0^3$ for $r = 2.14\ a_0$, while the experimental values for Q_1 and Q_2 are $-0.048\ ea_0$ and $-1.5\ ea_0^2$, respectively.[32,40] The problems associated with calculating the small dipole of CO reliably are well known.

At six equally spaced distances ranging from $R = 3$ to $8\ a_0$, Heitler–London energies for He–CO were computed at 15 relative orientations ranging from $\theta = 0$ to 180°. The results (in E_h) were then fitted to the form

$$E_{HL}^{(1)} = 10^{-3} \exp(a_0 - a_1 R + b_2 \cos^2\theta + b_3 \cos^3\theta) \sum_{\lambda=0}^{6} \sum_{p=0}^{3} a_p^{(\lambda)} R^p P_\lambda(\cos\theta) \tag{8}$$

yielding the values of the constants $\{a_i\}$, $\{b_i\}$, and $\{a_p^{(\lambda)}\}$ listed in the Appendix.

The present XC potential model for He–CO is based on one of several possible modifications[25,36,41,42] of an individually damped XC model developed[21,25] for isotropic rare-gas pairs. The form of the model for ΔE_C is common to all of the models, although the corrector function $G_{n_{max}}(R, \theta)$ depends on the number of multipolar energies included in the model.[25] Truncation of the sum in eqn. (4) at $n = 10$ is sufficient for systems such as He–CO which have 'mildly' divergent multipolar energy series.[21,25,43] In the atomic work, the model for the repulsive part of the XC potential was based on the first-order coulomb energy, which requires for its evaluation only the charge densities of the non-interacting monomers. Unfortunately, due to singularities in $E_C^{(1)}$, it is more difficult to apply this form to interactions involving molecules,[36] and so for molecular interactions the model for the (mainly) repulsive part of the potential energy is currently based on the first-order Heitler–London energy. However, studies of rare-gas interactions and preliminary work on other molecular systems do clearly indicate[36,41,42]

that the scaling function F in eqn. (2) will be a weak function of R and θ with values reasonably close to unity, which can in general be expressed as the type of double expansion used in eqn. (8).

In summary, the XC potential-energy model for He–CO is given by eqn. (2) and (4)–(8). The flexibility in the model is provided by varying the multipolar interaction coefficients $C_n^{(\lambda)}$ within their estimated uncertainties, and through varying parameters in the scaling function F. This type of flexibility, especially that associated with the $C_n^{(\lambda)}$s, has been instrumental in obtaining refined rare-gas pair potentials with high quality predictive abilities,[23,24,44] and is expected to be needed here. The 'starting' XC potential for He–CO, denoted XC(0), corresponds to fixing $F = 1$ in eqn. (2) and holding the $C_n^{(\lambda)}$ coefficients of eqn. (7) at the literature values given in the Appendix. Aside from system-specific input data, potential-energy models analogous to that developed here should be appropriate for all dispersion-dominated Rg–diatom interactions.

Optimized XC Potential-Energy Surface for He–CO

The essential character of the attractive well of our $F = 1$ starting potential, XC(0), is illustrated by plots of the angle dependence of the positions $R_e(\theta)$ and depths $\varepsilon(\theta)$ of its minima, shown as dashed curves in Fig. 1. Also seen are analogous plots for the empirical $V_{(3,3,3)}$ potential obtained in ref. 18 from ALS fits to the IR data (dotted curves), and for the *ab initio* TKD potential of Thomas *et al.*,[45] which has been used in numerous

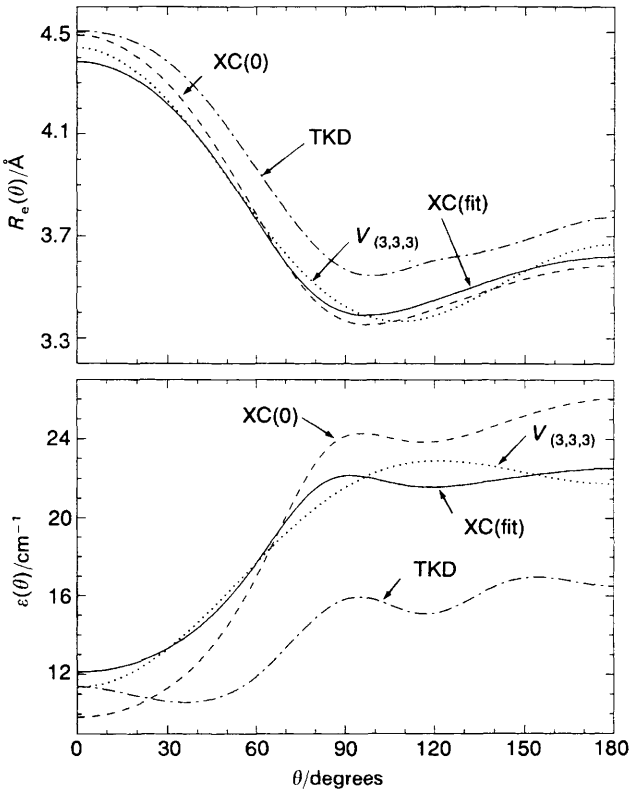

Fig. 1 Angle dependence of the depths and positions of the minima of various potential-energy surfaces for He–CO

calculations of line broadening and other collisional properties of this system (dot-dash curves). The well of this unmodified XC(0) potential is much more similar to that of the $V_{(3,3,3)}$ potential than to that of the earlier TKD surface. In particular, its larger overall well-depth means that it supports as many levels as the $V_{(3,3,3)}$ potential, while the pronounced asymmetry of this well-depth makes the relative intensities of the different types of lines[19] qualitatively correct. As a result, predictions based on it would have made it relatively easy to identify many of the observed transitions which could not be assigned prior to the spectral simulations described in ref. 19. This was not true for predictions based on the TKD potential.

To illustrate these last points, Fig. 2 compares the discrete IR spectrum of ^{4}He–CO predicted from the XC(0) potential [curve (*b*)], with that implied by the $V_{(3,3,3)}$ [inverted curve (*c*)]. In principle, it would be better to make comparison of this type directly with the raw experimental data. However, CO monomer lines obscure substantial portions of the bimer spectrum and, since the agreement with experiment for both the positions and intensities of the lines implied by the $V_{(3,3,3)}$ potential is, respectively, far better than and as good as the resolution of Fig. 2, it is more instructive to use the complete synthetic $V_{(3,3,3)}$ spectrum as a proxy for the experimental data. For the sake of comparison, Fig. 2(*a*) shows the synthetic spectrum implied by the TKD potential. While marked differences remain, the overall character of the spectrum implied by the XC(0) surface, which includes no adjusted parameters, is quite similar to the 'synthetic' experi-

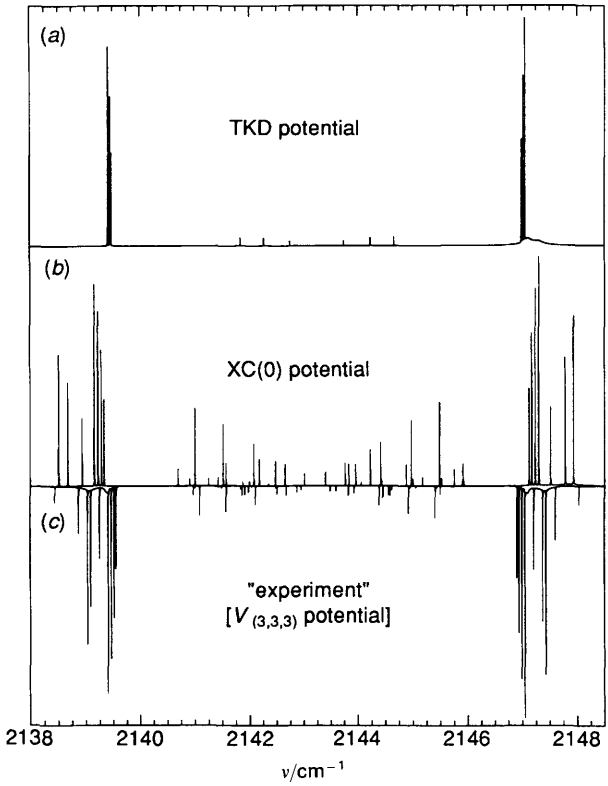

Fig. 2 Comparison of synthetic spectra for ^{4}He–CO generated from the indicated potential-energy surfaces

mental spectrum; this is clearly not true for the spectrum generated from the TKD surface.

The 'optimized' XC potential reported here was obtained from ALS fits to 27 experimental transition frequencies for ^{4}He–CO and 10 for ^{3}He–CO. For this data set, the high quality of the predictions based on the $V_{(3,3,3)}$ potential-energy surface is indicated by the modest RMSD value of 1.63 [recall that RMSD = 1 would mean that on average, the predictions agree with the observed line positions to within the latters' uncertainties of $u(Y_i) = 0.01$ cm^{-1}]. As discussed in ref. 18, the fact that this value is slightly larger than unity is not surprising, in view of the approximate way in which the dependence on the CO bond length was taken into account.

For this same data set, the RMSD value yielded by the starting XC(0) potential was 339. While this value may seem rather large, the good qualitative similarity between Fig. 2(*b*) and (*c*) suggests that modifying the potential to reduce it will not be difficult. Since part of the object of the present work has been to learn how to fit multidimensional XC potential surfaces to high-resolution spectral data, the results presented below were obtained from series of fits in which different sets of parameters were fixed and/or varied from one case to another. The resulting potential is thus only an interim version of an optimum XC potential for this system.

While the scaling function F is, in general, a (weak) function of both R and θ, in the present study it proved adequate to represent it as a function of θ only:

$$F = c_0 + c_1 P_1(\cos\theta) + c_2 P_2(\cos\theta) + c_3 P_3(\cos\theta) \tag{9}$$

where the c_λs are adjustable parameters. A key feature of the model is also allowing the $C_n^{(\lambda)}$ coefficients to vary within their estimated uncertainties. In the following, the results of these latter adjustments are represented by the scaling factors $R_n^{(\lambda)} = C_n^{(\lambda)}(\text{fitted})/C_n^{(\lambda)}(\text{initial})$, where $C_n^{(\lambda)}(\text{initial})$ are the starting values listed in the Appendix. Since the uncertainties in the literature values of the $C_n^{(\lambda)}$ coefficients in general increase with both n and λ, those corresponding to small n, λ were fixed at the starting values given in the Appendix, and some higher ones were allowed to vary subject to certain *ad hoc* constraints. In particular, our fits constrained $R_9^3 = R_9^1$ and $R_{10}^4 = R_{10}^0$. While these are not necessarily the optimal constraints, their use sufficed to reduce the number of free parameters while still allowing for considerable flexibility.

ALS fits of our XC model potential to the 37 experimental data, which varied the c_λ factors of eqn. (9) and certain of the $R_n^{(\lambda)}$ factors, as well as determining the additive band origin shift $\Delta\nu_0 = -0.00217$ cm^{-1}, yielded an RMSD of 1.80, a value very close to that for the $V_{(3,3,3)}$ surface of ref. 18. The resulting scaling factors are listed in Table 1; no uncertainties or correlation matrix are given for these constants, since this is an interim

Table 1 Dimensionless scaling parameters defining the determination of the present XC(fit) potential for He–CO from the starting XC(0) function; for (n, λ) combinations not listed here the factors R_n^λ all equal unity

λ	c_λ	$R_7^{(\lambda)}$	$R_8^{(\lambda)}$	$R_9^{(\lambda)}$	$R_{10}^{(\lambda)}$
0	0.976 96	—	1	—	0.928 36
1	−0.021 300	0.992 78	—	1.488 69	—
2	−0.073 860	—	1.224 58	—	0.804 28
3	−0.007 028 5	1	—	1.488 69	—
4	—	—	1	—	0.928 36

A Fortran subroutine for generating this potential is available.

result, and not a fully optimized version of the model. The values found for the c_λs confirm that F is indeed a weak function of θ, with its maximum deviations from unity being only -12.5% (at $\theta = 0°$) and $+1.4\%$ (at $\theta = 93°$). Note too that the adjustments required of the $R_n^{(\lambda)}$ coefficients are within the uncertainties in their initial values.

The angle dependence of the depths and positions of the minima of this fitted potential, XC(fit), are plotted as solid curves in Fig. 1. In view of the fact that XC(fit) and $V_{(3,3,3)}$ give essentially equivalent predictions for the experimental data, the qualitative differences between their $\varepsilon(\theta)$ plots is quite intriguing. It is interesting to note that the dip in $\varepsilon(\theta)$ near its maximum seen for XC(fit) also appeared in the *ab initio* TKD potential, and in a muted form, also in Hutson's potentials for Ar–HF and Ar–HCl.[7,8] At present, it cannot be said for certain whether or not this behaviour is real for He–CO. However, this difference does illustrate the sorts of discrepancies which can arise from model dependence in this type of analysis. Further comparisons among various potential-energy surfaces for this system are shown in Fig. 3, where cuts through the indicated potential-energy surfaces are shown at three representative angles. The XC(fit) potential is expected to be the most reliable in the extrapolation region associated with the upper segment of this figure.

As a final indication of the quality of the XC(fit) potential energy surface, Fig. 4 compares the predicted spectrum generated from it with that for the $V_{(3,3,3)}$ potential. The modest scaling introduced by the parameters given in Table 1 has clearly brought

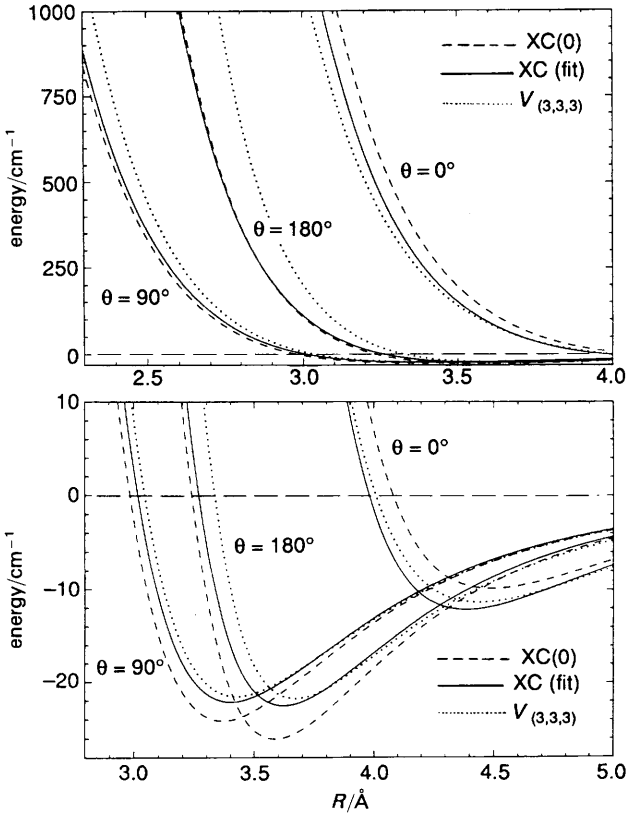

Fig. 3 Radial potential along cuts through various potential-energy surfaces for He–CO

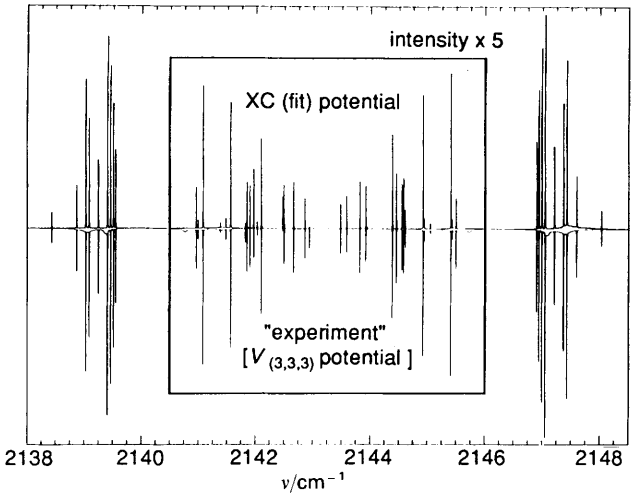

Fig. 4 Comparison of synthetic spectra for ^{4}He–CO generated from the indicated potential-energy surfaces; in the inner box, the intensity on the interval from 2140.5 to 2146.0 cm^{-1} is multiplied by a factor of five.

the relative intensities, as well as the line positions, yielded by the XC potential model into excellent agreement with experiment.

Discussion and Conclusions

The results presented show that an XC model for an anisotropic atom–diatom potential-energy surface can indeed match the ability of the best empirical potential to reproduce high-resolution experimental IR data. Moreover their sound theory-based form means that such fitted XC potentials can be expected to be relatively reliable in regions outside that sampled by the fitted experimental data. As discussed earlier, XC models are based on reasonably readily available input information, including a model for the (mostly) repulsive part of the potential that requires only isolated-monomer electronic wavefunctions. Thus, XC model potentials could well be the 'form-of-choice' for any interaction for which the requisite input information is available. Of course, other potential-energy models will also undoubtedly be useful for purposes analogous to those addressed here, if full use is made of the flexibility inherent in them.

It is important to realize that the flexibility built into the model, both through the adjustable parameters in the scale function F and through varying the multipolar energy coefficients $C_n^{(\lambda)}$ within their estimated uncertainties, is crucial to its successful application. The need for this flexibility is to be expected, since (i) the model employs the Heitler–London interaction energy evaluated using SCF, and not exact, monomer wavefunctions, (ii) the damping and corrector functions, which become significant as R decreases, are only approximately 'universal' and (iii) there are significant uncertainties inherent in the input multipolar energy coefficients for $n > 6$.

The 'interim' XC(fit) potential obtained here, which depends on four free and five constrained adjustable parameters, gives the same quality of fit to the IR data as is yielded by the 'empirical' $V_{(3,3,3)}$ potential of ref. 18, which depends on nine free parameters. The more realistic form of the XC potential helps to avoid the occurrence of non-physical parameters[41] such as have sometimes previously appeared in the fitting of IR data; for example, partly because the C_7^1 coefficient used in ref. 18 has an incorrect

sign, the effective $C_8(\theta)$ coefficient in the $V_{(3,3,3)}$ potential varies widely with angle and lacks the expected symmetry about $\theta = 90°$. The interim nature of the present XC(fit) potential is illustrated by the fact that it implies an isotropic dispersion coefficient ratio of $\chi \equiv C_{10}^{(0)}C_6^{(0)}/[C_8^{(0)}]^2 = 0.8896$, although for isotropic interactions, it is known that χ should have a value of approximately $1.2(\pm 0.1)$.[46] Using this condition as a constraint when fitting to the IR data would lead to a new XC potential for He–CO, and to a better understanding of this interaction.

In closing, it is interesting to note that there are significant differences between the wells of the XC(fit) and $V_{(3,3,3)}$ potentials (see Fig. 1 and 3), although both potentials explain the IR data to essentially the same high accuracy. This shows that IR data by itself will sometimes be unable to discriminate between potential-energy surfaces which appear to be quite different in the potential-well region. For He–CO this is, at least partly, due to the relatively large zero-point energy and small total number of bound levels. In any case, it is clear that other properties of the He–CO system must be taken into account in order to discriminate between XC(fit) and $V_{(3,3,3)}$ for most regions of configuration space, and hence to obtain a more definitive He–CO potential-energy surface.

We are very pleased to acknowledge helpful discussions with Prof. A. J. Thakkar and Drs. C. E. Chuaqui and R. J. Wheatley. Funding for this research has been provided through the Network of Centres of Excellence in Molecular and Interfacial Dynamics, supported by the Government of Canada.

Appendix

Constants defining the 'starting' XC(0) Potential for He–CO

As described earlier, the zero-adjustment $F = 1$ 'starting' XC(0) potential is defined by eqn. (2), with the mainly repulsive $E_{HL}^{(1)}$ function represented by eqn. (8) and the constants listed in Table A1. The initial values assumed for the composite (dispersion and induction) coefficients $C_n^{(\lambda)}$ of eqn. (7), with their estimated uncertainties, are then listed in Table A2, while the constants defining the damping functions of eqn. (6) are listed in Table A3.

Table A1 Constants defining the present algebraic representation of $E_{HL}^{(1)}$, as defined by eqn. (8) (in atomic units)

	$a_p^{(\lambda)}$			
λ	$p = 0$	$p = 1$	$p = 2$	$p = 3$
0	1	−0.551 802 6	0.207 437 6	−0.008 822 3
1	1.252 568 0	−1.099 283 2	0.286 126 0	−0.006 135 4
2	0.769 904 2	−0.432 171 2	0.129 332 3	—
3	0.033 302 89	−0.150 063 7	0.050 533 2	—
4	0.388 574 5	−0.102 120 0	0.009 251 5	—
5	0.271 424 8	−0.062 598 3	—	—
6	0.109 304 1	−0.023 570 8	—	—

$a_0 = 11.748\,904\,0$, $a_1 = 2.307\,097\,0$, $b_2 = 1.218\,159\,7$, $b_3 = -0.034\,257\,6$

Table A2 Values of the composite multipolar dispersion and induction coefficients $C_n^{(\lambda)}$ defining the mainly attractive part $\Delta E_C(R, \theta)$ of the starting XC(0) potential for He–CO *via* eqn. (4) and (7) (in atomic units)

	$C_n^{(\lambda)}$				
n	$\lambda = 0$	$\lambda = 1$	$\lambda = 2$	$\lambda = 3$	$\lambda = 4$
6	10.66532 (±1%)	—	0.98866 (±2%)	—	—
7	—	29.04352 (±30%)	—	−0.34893 (±30%)	—
8	268.2192 (±15%)	—	281.7367 (±30%)	—	−5.0400 (±50%)
9	—	1240 (±50%)	—	61.27 (±50%)	—
10	6464 (±50%)	—	10050 (±60%)	—	1980 (±70%)

Table A3 Values of the A_n, B_n and C_n constants characterizing the damping functions $f_n(R, \theta)$ of eqn. (6), as taken from ref. 28 (in atomic units)

n	A_n	B_n	D_n
6	0.364 8	0.033 60	0.001 651
7	0.327 8	0.030 09	0.000 935 9
8	0.307 3	0.024 69	0.001 227
9	0.265 584	0.027 943 2	0.000 394 797
10	0.251 4	0.023 79	0.000 566 4

References

1 A. Watanabe and H. L. Welsh, *Phys. Rev. Lett.*, 1964, **13**, 810.
2 R. G. Gordon and J. K. Cashion, *J. Chem. Phys.*, 1966, **44**, 1190.
3 J. K. Cashion, *J. Chem. Phys.*, 1966, **45**, 1656.
4 R. J. Le Roy and J. van Kranendonk, *J. Chem. Phys.*, 1974, **61**, 4750.
5 R. J. Le Roy and J. M. Hutson, *J. Chem. Phys.*, 1987, **86**, 837.
6 J. M. Bowman, B. Gazdy, P. Schafer and M. C. Heaven, *J. Phys. Chem.*, 1990, **94**, 2226.
7 J. M. Hutson, *J. Phys. Chem.*, 1992, **96**, 4237.
8 J. M. Hutson, *J. Chem. Phys.*, 1992, **96**, 6752.
9 R. C. Cohen and R. J. Saykally, *J. Chem. Phys.*, 1993, **98**, 6007.
10 L. Beneventi, P. Casavecchia, G. G. Volpi, C. R. Bieler and K. C. Janda, *J. Chem. Phys.*, 1993, **98**, 178.
11 J. Tennyson, *Comput. Phys. Rep.*, 1986, **4**, 1; A. G. Ayllón, J. Santamaría, S. Miller and J. Tennyson, *Mol. Phys.*, 1990, **71**, 1043.
12 A. C. Peet and W. Yang, *J. Chem. Phys.*, 1989, **90**, 1746.
13 T. Slee and R. J. Le Roy, *J. Chem. Phys.*, 1993, **99**, 360.
14 M. J. Bramley and T. Carrington Jr, *J. Chem. Phys.*, 1993, **99**, 8519, 8541.
15 T. Slee, R. J. Le Roy and C. E. Chuaqui, *Mol. Phys.*, 1992, **77**, 111.
16 R. J. Beamish, P. A. Block, L. G. Pederson, W. Yang and R. E. Miller, *J. Chem. Phys.*, 1993, **99**, 8585.
17 W. Jäger, M. C. L. Gerry, C. Bissonnette and F. R. W. McCourt, *Faraday Discuss.*, 1994, **97**, 105.
18 C. E. Chuaqui, R. J. Le Roy and A. R. W. McKellar, *J. Chem. Phys.*, 1994, **101**, in the press.
19 R. T. Pack, *Chem. Phys. Lett.*, 1978, **55**, 197.
20 K.-C. Ng, W. J. Meath and A. R. Allnatt, *Chem. Phys.*, 1978, **32**, 175; *Mol. Phys.*, 1979, **37**, 237.
21 W. J. Meath, D. J. Margoliash, B. L. Jhanwar, A. Koide and G. D. Zeiss, in *Intermolecular Forces* (Proceedings of the 14th Jerusalem Symposium on Quantum Chemistry and Biochemistry), ed. B. Pullman, Reidel, Dordrecht, 1981, pp. 101–115.
22 J. Hepburn, G. Scoles and R. Penco, *Chem. Phys. Lett.*, 1975, **36**, 451; R. Ahlrichs, R. Penco and G. Scoles, *Chem. Phys.*, 1977, **19**, 119; C. Douketis, G. Scoles, S. Marchetti, M. Zen and A. J. Thakker, *J. Chem. Phys.*, 1978, **76**, 3057.
23 R. A. Aziz, in *Inert Gases – Potentials, Dynamics and Energy Transfer in Doped Crystals*, ed. M. L. Klein, Springer Verlag, Berlin, 1984, ch. 2.
24 R. A. Aziz, M. J. Slaman, A. Koide, A. R. Allnatt and W. J. Meath, *Mol. Phys.*, 1992, **77**, 321; A. K. Dham, W. J. Meath, A. R. Allnatt, R. A. Aziz and M. J. Slaman, *Chem. Phys.*, 1990, **142**, 173; R. A. Aziz and M. J. Slaman, *Mol. Phys.*, 1986, **58**, 679; and references therein.
25 W. J. Meath and M. Koulis, *J. Mol. Structr.*, 1991, **226**, 1 and references therein.
26 K. T. Tang and J. P. Toennies, *J. Chem. Phys.*, 1977, **66**, 1496; 1984, **80**, 3726.
27 H. Kreek and W. J. Meath, *J. Chem. Phys.*, 1969, **50**, 2289.
28 A. Koide, W. J. Meath and A. R. Allnatt, *Chem. Phys.*, 1981, **58**, 105.
29 M. Bulski, P. E. S. Wormer and A. van der Avoird, *J. Chem. Phys.*, 1991, **94**, 8096 and references therein.
30 H. Hettema, P. E. S. Wormer and A. J. Thakkar, *Mol. Phys.*, 1993, **76**, 533.
31 B. L. Jhanwar and W. J. Meath, *Chem. Phys.*, 1982 **67**, 185; W. J. Meath and A. Kumar, *Int. J. Quantum Chem.*, 1990, **24**, 501; A. Kumar and W. J. Meath, unpublished work.
32 J. S. Muenter, *J. Mol. Spectrosc.*, 1975, **55**, 490.
33 W. Rijks and P. E. S. Wormer, *J. Chem. Phys.*, 1989, **90**, 6507.
34 R. D. Amos and J. E. Rice, CADPAC-the Cambridge Analytic Derivatives Package, Issue 4.0, 1987.
35 I. C. Hayes and A. J. Stone, *Mol. Phys.*, 1984, **53**, 69, 83.
36 R. J. Wheatley and W. J. Meath, *Mol. Phys.*, 1993, **79**, 253.

37 M. W. Schmidt and K. Ruedenberg, *J. Chem. Phys.*, 1979, **71**, 3951.
38 F. B. van Duijneveldt, *IBM Research Report RJ945*, 1971.
39 P. A. Christiansen and E. A. McCullough, *J. Chem. Phys.*, 1977, **67**, 1877.
40 W. L. Meerts, F. H. DeLeeuw and A. Dymanus, *Chem. Phys.*, 1977, **22**, 319.
41 W. J. Meath, in *Atomic Physics and Quantum Optics*, ed. H. A. Bachor, K. Kumar and B. A. Robson, World Scientific Press, 1993, pp. 157–213.
42 M. Koulis, T. H. Wu, A. K. Dham, R. J. Wheatley, A. R. Allnatt and W. J. Meath, unpublished work.
43 R. A. Aziz, W. J. Meath and A. R. Allnatt, *Chem. Phys.*, 1983, **78**, 295.
44 R. A. Aziz and H. H. Chen, *J. Chem. Phys.*, 1977, **67**, 5719; R. A. Aziz, *Mol. Phys.*, 1979, **38**, 177; A. Koide, W. J. Meath and A. R. Allnatt, *Mol. Phys.*, 1980, **39**, 895.
45 L. D. Thomas, W. P. Kraemer and G. H. F. Diercksen, *Chem. Phys.*, 1980, **51**, 131.
46 R. J. Le Roy, *Can. J. Phys.*, 1974, **52**, 246; A. J. Thakker and V. H. Smith Jr., *J. Phys. B*, 1974, **7**, L321; F. Mulder, G. F. Thomas and W. J. Meath, *Mol. Phys.*, 1980, **41**, 249.

Paper 4/00458B; *Received* 21*st January*, 1994